ORIGINAL ARTICLE

A cross-standardized flow cytometry platform to assess phenotypic stability in precursor B-cell acute lymphoblastic leukemia (B-ALL) xenografts

Nina Rolf MD, PhD[1,2] | Lorraine Y. T. Liu[3] | Angela Tsang[3] |
Philipp F. Lange PhD[1,4] | Chinten James Lim PhD[1,2] |
Christopher A. Maxwell PhD[1,2] | Suzanne M. Vercauteren MD, PhD[3,4] |
Gregor S. D. Reid PhD[1,2]

[1]Michael Cuccione Childhood Cancer Research Program, BC Children's Hospital Research Institute, University of British Columbia, Vancouver, British Columbia, Canada

[2]Department of Pediatrics, University of British Columbia, Vancouver, British Columbia, Canada

[3]Clinical Immunology Lab, Division of Hematopathology, BC Children's Hospital, Vancouver, British Columbia, Canada

[4]Department of Pathology and Laboratory Medicine, University of British Columbia, Vancouver, British Columbia, Canada

Correspondence
Nina Rolf, BC Children's Hospital Research Institute, Michael Cuccione Childhood Cancer Research Program, 950 West 28th Avenue, Room 3062, Vancouver, BC V5Z 4H4, Canada.
Email: ninarolf@mail.com

Funding information
BC Children's Hospital Foundation, Clinical & Translational Research Seed Grant (N.R.); Children's & Women's Hospital Vancouver, Pathology Seed Grant (S.M.V); Michael Cuccione Foundation BRAvE Initiative; Canadian Institutes of Health Research (CIHR), Grant/Award Number: Fellowship Grant (N.R.): 223877; Leukemia and Lymphoma Society of Canada, Operating Grant (G.R.), Grant/Award Number: 430741

Abstract

With the continued poor outcome of relapsed acute lymphoblastic leukemia (ALL), new patient-specific approaches for disease progression monitoring and therapeutic intervention are urgently needed. Patient-derived xenografts (PDX) of primary ALL in immune-deficient mice have become a powerful tool for studying leukemia biology and therapy response. In PDX mice, the immunophenotype of the patient's leukemia is commonly believed to be stably propagated. In patients, however, the surface marker expression profile of the leukemic population often displays poorly understood immunophenotypic shifts during chemotherapy and ALL progression. We therefore developed a translational flow cytometry platform to study whether the patient-specific immunophenotype is faithfully recapitulated in PDX mice. To enable valid assessment of immunophenotypic stability and subpopulation complexity of the patient's leukemia after xenotransplantation, we comprehensively immunophenotyped diagnostic B-ALL from children and their matched PDX using identical, clinically standardized flow protocols and instrument settings. This cross-standardized approach ensured longitudinal stability and cross-platform comparability of marker expression intensity at high phenotyping depth. This analysis revealed readily detectable changes to the patient leukemia-associated immunophenotype (LAIP) after xenotransplantation. To further investigate the mechanism underlying these complex immunophenotypic

shifts, we applied an integrated analytical approach that combined clinical phenotyping depth and high analytical sensitivity with unbiased high-dimensional algorithm-based analysis. This high-resolution analysis revealed that xenotransplantation achieves patient-specific propagation of phenotypically stable B-ALL subpopulations and that the immunophenotypic shifts observed at the level of bulk leukemia were consistent with changes in underlying subpopulation abundance. By incorporating the immunophenotypic complexity of leukemic populations, this novel cross-standardized analytical platform could greatly expand the utility of PDX for investigating ALL progression biology and assessing therapies directed at eliminating relapse-driving leukemic subpopulations.

KEYWORDS

acute lymphoblastic leukemia, diagnostic leukemia, heterogeneity, high-dimensional flow analysis, immunophenotypic shift, leukemia-associated immunophenotype, patient-derived xenotransplantation, PDX model, recapitulate, subpopulation complexity

1 | INTRODUCTION

Acute lymphoblastic leukemia (ALL) exhibits considerable clonal heterogeneity at diagnosis (DX) [1–5]. Relapses, which are mostly driven by outgrowth of minor diagnostic subpopulations [2, 3, 6–10], continue to be associated with poor outcomes [11–13]. Patient-derived xenografts (PDX), in which immune-deficient mice are engrafted with primary ALL cells, have emerged as an important source of leukemia progression and drug sensitivity data that could inform the development of much needed new therapies [2, 14–27]. The significant potential of ALL-PDX as screening platforms for clinical trials and for personalized precision medicine approaches critically depends on their ability to recapitulate clinical disease [17, 22, 28, 29], and there is accumulating evidence that many aspects of the morphologic, genomic, transcriptomic, epigenetic, and proteomic landscapes of primary ALL are maintained in the PDX setting [2, 4, 14, 19, 20, 27, 30, 31].

The ability of ALL-PDX to recapitulate patient-specific leukemia immunophenotypes is less established. As several PDX studies reported selected antigen expression levels that are typical for ALL on xenografted leukemia [14, 19, 20], it is commonly assumed that the patient's immunophenotype is stably propagated after xenotransplantation [4, 27]. In patients with precursor B-cell ALL (B-ALL), however, the leukemia-associated immunophenotypic pattern (LAIP), defined by asynchronous or aberrant expression of B-cell differentiation markers on the bulk leukemic population, rarely remains stable [32–38]. At diagnosis (DX), B-ALL commonly shows heterogeneous expression of a variety of surface antigens on the leukemic population [32, 36, 38–40], and exhibits unpredictable immunophenotypic shifts during chemotherapy [32, 37, 38, 41, 42] and disease progression [32, 33, 35, 38, 40, 43–46]. The term immunophenotypic shift is commonly used in clinical medicine when the expression intensity of one or several surface markers on the leukemic population is modulated to a varying degree; interpretation of these fluctuations continues to pose significant hurdles in clinical immunophenotyping efforts [33,

36, 38]. Although the underlying mechanisms are not fully understood [32, 33, 35, 38, 40, 46], phenotypic heterogeneity and immunophenotypic shifts may have important implications for the assessment of reservoirs of leukemia involved in drug resistance and evolution of relapse [9, 39, 47].

In clinical flow-based diagnostics, rigorous standardization is paramount for enabling reproducible comparison of marker expression intensity across different samples, patients, flow cytometers, and time [36, 38, 41, 48–56]. This ensures accurate and reliable distinction of B-ALL from normal hematopoietic cell lineages, and is of particular importance in measurable residual disease (MRD) diagnostics at the end of induction chemotherapy, where the phenotypic shifts, strong recovery of normal hematopoiesis, and low leukemic blast count further complicates consistent assessment of leukemia persistence in the patient [33, 34, 38, 40, 46, 57]. In contrast, the propensity of PDX mice to exclusively expand ALL blasts provides phenotypic and functional clarity of the xenotransplanted leukemia [8, 14, 16, 21, 23, 26, 47, 58, 59].

To more rigorously assess phenotypic stability after xenotransplantation, we comprehensively immunophenotyped B-ALL from matched patient- and xenograft-derived samples using the identical, clinically standardized flow protocols and instrument settings. To exclude the possibility of chemotherapy inducing any immunophenotypic shifts of the patient LAIP, we focused on xenotransplanting primary leukemia from time of initial diagnosis (pre-therapy). By performing a cross-standardized analysis at high phenotyping depth, we investigated whether complex immunophenotypic shifts of the patient LAIP do occur after xenotransplantation, which would significantly expand our current understanding of phenotypic stability in ALL-PDX mice. To overcome the limitations of conventional approaches to investigating the multi-dimensionality of phenotypic complexity [60–62], we developed an integrated analysis method that successfully resolved the same subpopulation complexity in matched samples by discriminating their

stable high-dimensional marker profiles. Our results demonstrate that xenotransplantation achieves propagation of phenotypically stable B-ALL subpopulations, albeit at different abundance levels.

We here present the methodological principles embedded in our translational platform and the step-wise application of the various components of our workflow to study whether xenotransplantation faithfully recapitulates the patient-specific immunophenotype. Our results highlight that by achieving cross-standardized assessment of matched patient- and xenotransplanted samples, subpopulation-specific analyses are feasible, which could greatly increase the utility of ALL-PDX mice to study LAIP shifts during disease progression and to successfully monitor the trajectories of phenotypically defined leukemic subpopulations.

2 | METHODS

2.1 | Clinical B-ALL samples

Bone marrow (BM) samples were collected at time of DX from pediatric precursor B-cell ALL (B-ALL) patients by fine needle aspiration in sodium citrate tubes and distributed to the relevant clinical laboratories at BC Children's Hospital and the BC Children's Hospital Biobank. Cryopreserved aliquots of de-identified B-ALL BM mononuclear cells (MNCs) and associated patient and disease information were obtained for this study from the Biobank. Clinical characteristics for each patient are shown in Table S1. Informed consent from human subjects was obtained in all cases in accordance with the Declaration of Helsinki and the study was performed under the University of British Columbia Children's & Women's Research Ethics Board-approved protocols (H14-02930).

2.2 | Patient-derived leukemia xenografts

Briefly, non-preconditioned 6- to 10-week-old NOD.Cg-Prkdcscid/IL2rgtm1Wjl/SzJ (NSG) mice (Jackson Laboratory) were injected via tail vein with $1–5 \times 10^5$ freshly thawed, viable diagnostic B-ALL BM-MNCs in 0.2 ml phosphate-buffered saline. Recipients, termed DX-PDX, were followed for up to 6 months with regular peripheral blood monitoring to detect human CD19, CD45, and HLA-ABC positive cells using a routine translational flow cytometry panel (Table S2) and data acquisition with Fortessa X-20 (BD Biosciences). Upon onset of overt leukemia or at 6-month endpoint, BM and spleen cells were harvested and samples were analyzed by multi-parameter flow cytometry within 24 h with the identical 10-color clinical flow panel (Table S2) and cross-standardized flow protocols as used for the diagnostic work-up in the patient. Non-injected NSG control mice analyzed with the same 10-color clinical flow panel (Table S2) demonstrated negligible background staining, which was confirmed with an anti-murine CD45-containing research B-ALL flow panel (Table S2, Figure S1). As expected [14, 22, 24, 28], non-preconditioned NSG recipient mice exclusively expand B-ALL cells and no non-B cell lineage human cells

were detected in any PDX using various translational flow panels (Table S2) and data acquisition with Fortessa X-20. All experiments were conducted in accordance with a University of British Columbia Animal Care-approved protocol (A19-0197).

2.3 | Clinical immunophenotyping of diagnostic B-ALL

Diagnostic BM from children with B-ALL were immunophenotyped within 24 h in BC Children's Hospital Hematopathology flow laboratory as part of routine patient care using a clinically standardized, 10-color monoclonal antibody combination designed to distinguish the LAIP of B-ALL blasts from normal hematopoietic cells (Table S2; Supporting Information, Clinical cell staining). All steps were performed in strict adherence to clinical standard operating procedures (SOP) to ensure quality-controlled assessments [36, 51, 55, 56]. Optimal instrument alignment, fluidics, and voltages setup of the Navios flow cytometer (Beckman Coulter, Indiana, IN, United States) included standardization with Flow Check Pro and Flow Set Pro Fluorospheres (Beckman Coulter) as per clinical SOP, and stable marker expression intensity, which ensured longitudinal comparability of flow results, was verified by consistently achieving the pre-determined optimal target values during daily quality control. Antibody lots were tested for fluorescence variation [49] and each new antibody cocktail verified to maintain staining characteristics.

To achieve the same clinical immunophenotyping depth and enable direct comparison of marker expression intensity across platform, all PDX-derived diagnostic B-ALL samples were stained with the identical clinical flow protocols (Table S2) following the same SOPs and acquired with the same Navios flow cytometer model with cross-standardized instrument settings. For each sample, between 1×10^5 and 1×10^6 events were collected, depending on the analytical sensitivity required for rare event detection (Supporting Information, Analytical assay sensitivity).

2.4 | Comprehensive clinical gating

Clinically acquired list mode data (LMD) files were analyzed using Kaluza software (Version 1.2, Beckman Coulter). The same multi-step manual gating method, termed "integrated LAIP-based Different-from-Normal" [63], was consistently applied to identify B-ALL blast populations in every sample from patients and PDX mice. Samples analyzed this way are referred to as "clinically gated." The comprehensive clinical gating approach followed published principles of B-ALL immunophenotyping [33, 35, 38, 40, 46]. Briefly, after routine exclusion of air bubbles, debris, aggregated and dead cells, the patient-specific LAIP was manually identified among viable MNCs (or viable nucleated singlets in PDX samples) by expert operators following a pre-defined gating hierarchy on sequential two-dimensional dot plots (Figure S2A). The patient-specific LAIP is used to discriminate B-ALL blasts from healthy precursor B cells using different-from-

normal gating, where the differentiation and maturation patterns of normal progenitor B cells in BM are represented within the pre-established B cell maturation matrix shown as contour plots (Figure S2B) [57, 64]. As the specific pattern of immunophenotypic aberrancies can differ significantly between each leukemia [32, 37, 41, 42, 65], patient-specific fine-tuning of LAIP-based gating is essential.

2.5 | Unbiased algorithm-based high-dimensionality reduction analysis

To explore multi-dimensional relationships that might not be fully captured by the manual analysis of sequential two-dimensional dot plots [61, 66, 67], we used t-distributed stochastic neighbor embedding (t-SNE) [68], an unbiased, high-dimensionality reduction computational algorithm (Supporting Information, t-SNE analysis). As we chose to use FlowJo™ software (Ashland, OR, United States) with their user-friendly plugins for high-dimensional analysis, we first confirmed that the FlowJo-based clinical gating strategy recapitulated the exact identification of the patient-specific blast population obtained with the Kaluza®-based clinical gating (data not shown). Unbiased high-dimensional t-SNE maps of 30,000–50,000 total viable nucleated xenograft BM singlets were generated to: (i) identify low-level residual human blast cells from mouse background in DX-PDX; (ii) to rule out non-specific background staining of murine cells with human markers in non-injected NSG control mice (Figure S1); and (iii) to verify the absence of phenotypically normal lymphoid or myeloid cell lineages. For subpopulation-specific analyses, we downsampled 30,000–50,000 B-ALL blasts from the clinically gated leukemic population and created individual tSNE maps using the differentially expressed markers (6–8 markers), which had to be identical in matched samples. For all t-SNE analyses, we ran the FlowJo®-embedded plug-in (v10.4.2) with the standard settings of 1000–2000 iterations, 20–40 perplexity, 200 eta and 0.5 theta. We repeated each analysis several times to ensure that a stable configuration of the t-SNE map was indeed achieved. Heat maps of marker intensity were overlaid with each t-SNE map to visualize the full marker expression pattern and to verify the immunophenotypic pattern at the single cell level.

2.6 | Integrated analysis of phenotypic shifts and leukemic subpopulations

Our integrated analysis leveraged the immunophenotypic clarity of xenograft-expanded leukemia (bestowed by absence of normal human hematopoietic cells), the high analytical sensitivity and phenotyping depth of clinical MRD methodology, and the unbiased high-dimensional algorithm-based analysis. This unsupervised analytic approach enabled the resolution of phenotypically distinct leukemic subpopulations in PDX that matched the heterogeneous expression patterns of the same markers in the entire leukemic population (Supporting Information, Sub-populations). We then re-analyzed the clinical flow data using this approach. All t-SNE based subpopulations were subsequently visualized

on N × N views of conventional two-dimensional dot plots and histogram overlays to verify their distinct immunophenotypic pattern, sustained separation and concise population characteristics in all N × N views. Likewise, manually gated populations had to show clear separation with one or more surface markers on two-conventional dot plots, while sustaining concise population characteristics in all N × N views and presenting as spatially resolved populations with matched location on the unsupervised t-SNE map. Results generated with both approaches had to match numerically and phenotypically.

3 | RESULTS

3.1 | Standardized comprehensive phenotyping reveals immunophenotypic shifts after xenotransplantation

Our translational analytical flow platform was designed to achieve identical clinical immunophenotyping in cross-standardized settings, which ensured the stability of marker expression intensity across platform and inter-sample comparability at the same phenotyping depth. To assess marker-specific shifts after xenotransplantation, we first overlaid B-ALL populations from the PDX (DX-PDX) and corresponding patient (DX), which had been identically gated (Figure 1A) using the comprehensive clinical gating approach (Figure S2), as conventional histograms (Supporting Information, Conventional histogram overlays). For a representative sample (BB008), both CD19 and CD45 expression intensity showed a homogenous histogram peak, typical for a large, dominant population (Figure 1B) [32, 38, 39]. However, while peak intensity of CD19 expression was identical between DX-PDX and DX, CD45 expression was decreased by more than half a log after xenotransplantation. As our standardized platform enables direct comparison of marker expression intensity, this decrease in expression intensity mirrors the gradual loss in CD45 expression frequently observed in patients during the course of their disease [32]. Expression intensity of 5 out of 6 additional markers was either notably increased or decreased in DX-PDX mice (Figure 1C). CD34 was most prominently gained after xenotransplantation, which was accompanied by a shift from a heterogeneous expression pattern in the patient to a homogenous expression pattern in DX-PDX. Also, the change in expression of the various B-cell differentiation markers (CD10, CD20, CD34 and CD38) was not coordinated in a manner that could indicate a switch to a more mature or immature B-ALL phenotype [32]. Although these changes in expression intensity are moderate, as no marker was entirely lost or newly gained, they are consistent with a complex, multi-dimensional immunophenotypic shift of the patient's leukemia after xenotransplantation.

3.2 | An integrated analysis approach enhances subpopulation detection

As immunophenotypic shifts could be the result of changes in marker expression of the entire leukemic population or in the relative
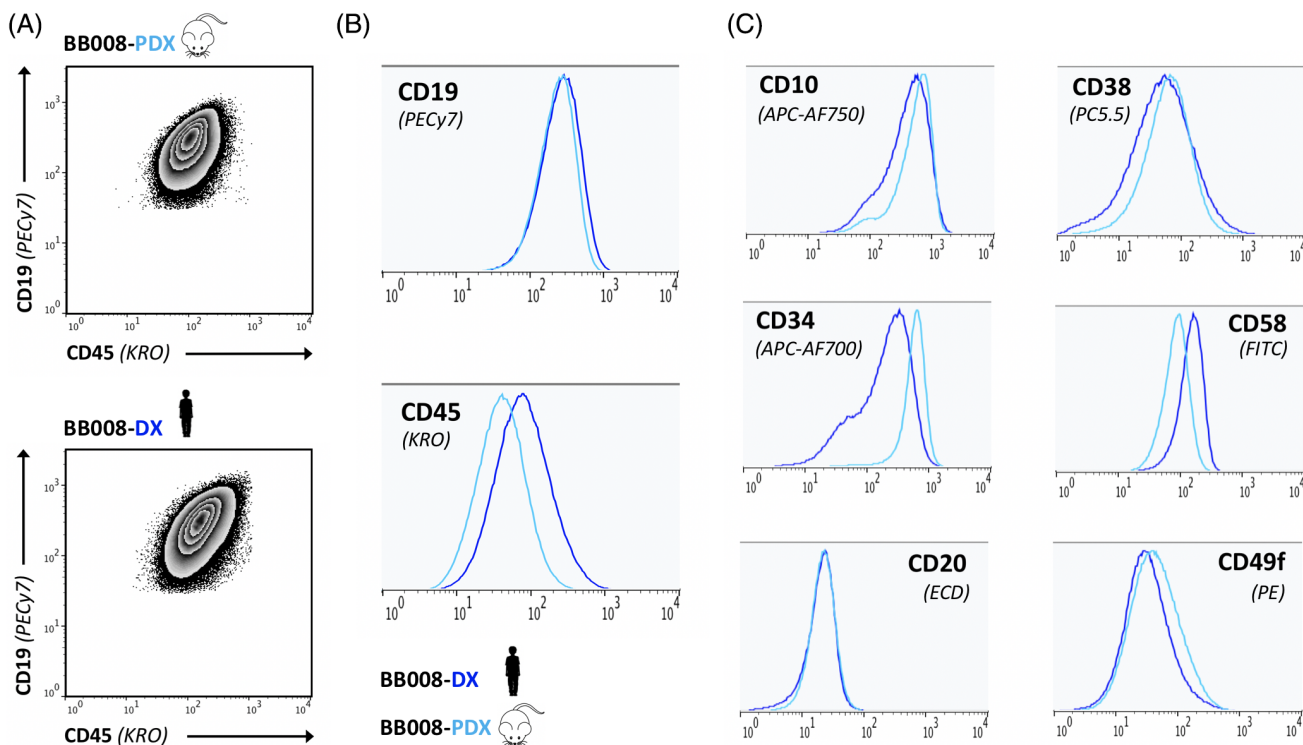
FIGURE 1 Staining characteristics of identically phenotyped xenograft- and patient-derived leukemia using cross-standardized settings. Clinically gated xenograft (DX-patient-derived xenograft [PDX]) or patient (DX) leukemic populations from patient BB008 are shown (A) as density plots (5% zebra plot, outliers as individual dots) on two-dimensional plots depicting anti-human CD19 versus anti-human CD45 staining intensities, or (B + C) as histogram overlays to better facilitate direct comparison of marker expression intensity showing (B) only the B-cell lineage marker (CD19) and hematopoietic marker (CD45) compared to (C) the panel's high phenotyping depth. The rigorous cross-standardization of our translational approach ensured the stability of marker expression intensity across platform and inter-sample comparability at the same comprehensive phenotyping depth [Color figure can be viewed at wileyonlinelibrary.com]

abundance of phenotypically distinct leukemic subpopulations, we further investigated the mechanism underlying the observed shift after xenotransplantation. As the heterogeneous expression patterns of CD10 and CD34 (Figure 1C) suggested that subpopulation complexity was not fully captured by histogram representations, we evaluated whether phenotypically distinct subpopulations were present at high-resolution. Histograms possess a well-known visualization bias toward dominant populations (Figure S3A), rendering subpopulations as heterogeneous histogram distributions only when present at >10% and as two distinct peaks (bimodal) only when co-dominant [32, 38–40]. When plotting the xenografted leukemia (DX-PDX) as density plots with all outliers as individual dots to visualize their complete population characteristics on N × N views (representative examples shown in Figure S3B), it revealed considerable phenotypic complexity (Figure 2A) that extended beyond the heterogeneous histogram representations (Figure 1C).

In order to distinguish distinct leukemic subpopulations within the entire B-ALL population, their differential expression patterns, often of the same markers, need to be identified. Yet, the multi-dimensionality of this complex immunophenotype (Figure 2A) underscores the well-known challenges that complex high-dimensional data pose for manually establishing a sequential gating approach [60–62,

67, 69]. Identifying distinct marker expression patterns in this context heavily relies on adequate data visualization by expert users to identify the best manual gating approach [48, 61, 67, 70]. By choosing the two-dimensional plots with the most prominent subpopulation characteristics, we manually established a conventional sequential gating strategy for BB008 that identified two clearly CD10-separated subpopulations (Figure 2B), which were further separated into two additional subpopulations by their distinct CD34/CD38 expression pattern; each time falling within the identical gates (Figure 2C + D). As required by our strict subpopulation criteria (Supporting Information, Subpopulation criteria), all four subpopulations showed good immunophenotypic separation and clustering on various two-dimensional plots (representative example shown in Figure 2E).

To more fully explore the multi-dimensional relationships present in our data without introducing a potential gating bias [60, 61, 67], we integrated the unsupervised t-SNE algorithm into the conventional gating approach [68]. As we had previously downsampled the total event count to 30,000 blast cells to perform all analyses on the identical population, cross-validation between both approaches was feasible. When the manually identified subpopulations were overlaid with the unbiased t-SNE map, all four DX-PDX subpopulations constituted distinct and spatially resolved populations in the high-dimensional
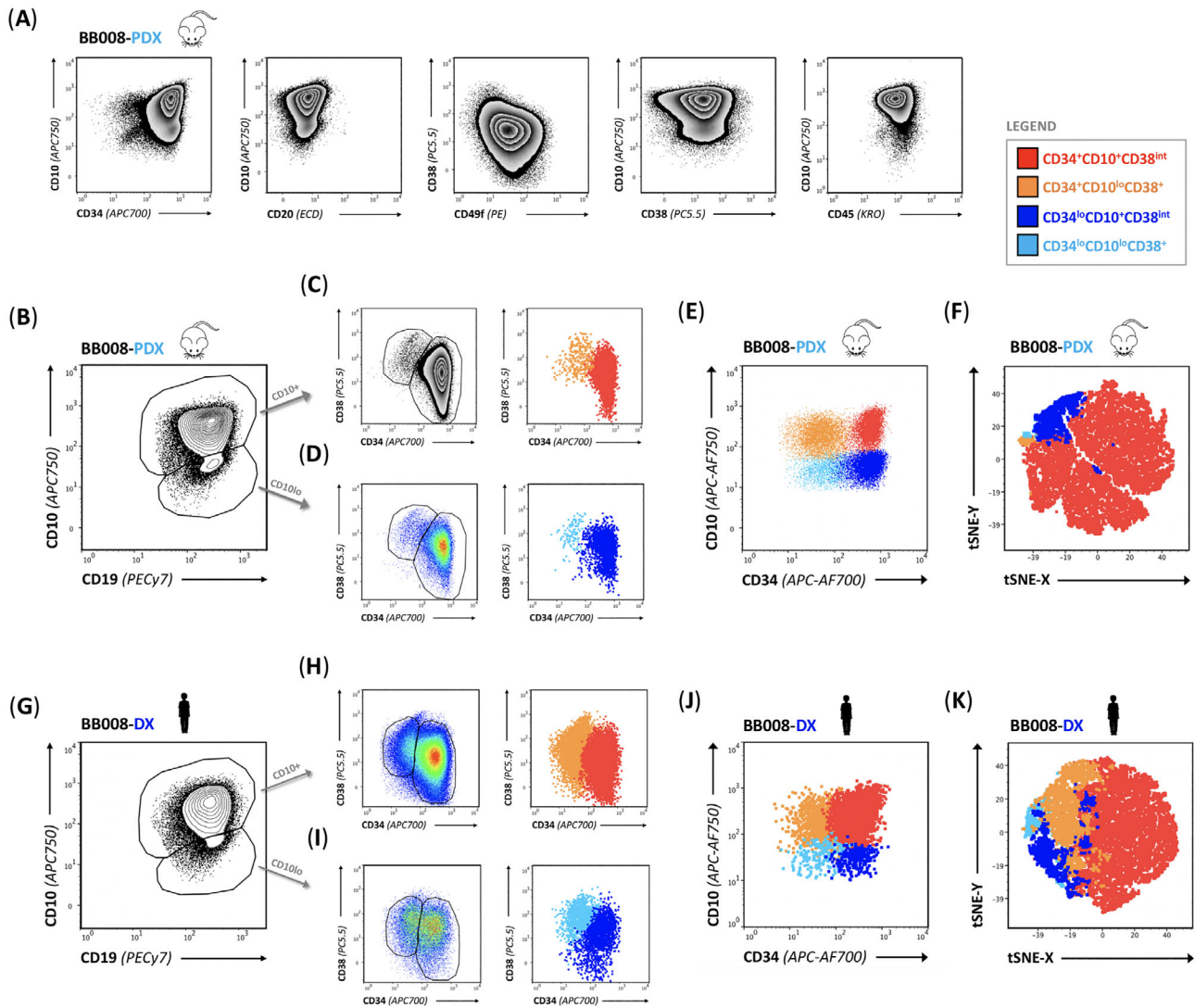
FIGURE 2 Manually identifying population characteristics indicative of leukemic subpopulations. (A) Density plots (5% zebra plot, outliers as individual dots) of the clinically gated leukemic population of DX-patient-derived xenograft (PDX), when visualized at greater immunophenotyping depth, better resolve low-frequency information that extend beyond dominant population characteristics. The varying phenotypic heterogeneity on various two-dimensional plots suggests presence of a complex immunophenotype. (B–K) Patient-specific manual gating strategy of sequential two-dimensional dot plots, identically applied in DX-PDX (B–D) and the patient (DX) (H–I), resolve the same phenotypically distinct leukemic subpopulations in both settings. The identified four subpopulations were color-coded according to their distinct phenotype and simultaneously visualized on N × N plots (representative CD10/CD34 plots shown) confirming that the gating approach had identified authentic population characteristics (E + J). Of note, the different magnitude of each subpopulation within the total leukemic population impacts the visual representation of subpopulations. For each case, all leukemia-specific analyses were performed on the identical leukemic population, downsampled to 30,000 blasts each, to ensure cross-validation between the conventional manual gating (B–D; G–I) and the high-dimensional gating (F + K) approach. Overlay of manually gated subpopulations onto the respective unsupervised dimension-reduced t-SNE map depicts their concise clustering within the high-dimensional population characteristics, their relative abundance, and gating accuracy at the single cell level (F + K) [Color figure can be viewed at wileyonlinelibrary.com]

space (Figure 2F), yet with some gating inconsistencies at the single cell level. Applying the same manual gating strategy in the independent analysis of the corresponding patient leukemia (DX) identified the same subpopulation complexity (Figure 2G–I). All four manually gated subpopulations showed decent immunophenotypic separation and clustering in all N × N density plots (representative plot shown in Figure 2J). When visualized in the high-dimensional t-SNE space, however, their gating precision at the single-cell level was even less accurate than in the DX-PDX (Figure 2K), highlighting the difficulties

of clearly discriminating complex expression patterns in the two-dimensional space.

3.3 | Unbiased high-dimensional t-SNE analysis confirms the stable propagation of subpopulations

Since unbiased t-SNE analysis automatically separates cells into spatially resolved populations on the dimension-reduced t-SNE map based

on the totality of markers they express, this leads to better separation of distinct cell populations in the multi-dimensional space [61, 67]. As demonstrated in Figure 3A (identical t-SNE map as in Figure 2F), unsupervised t-SNE analysis of DX-PDX successfully identified the phenotypes of the same four subpopulations (marker expression heatmaps), as well as their clear separation in the multi-dimensional space of the t-SNE map. As t-SNE analysis is unbiased and does not rely

on the manual sequential gating of the conventional approach, their multi-dimensional separation facilitates superior gating precision and independently verifies their accurate identification (Figure 3A). By utilizing the high analytical sensitivity of clinical MRD methodology (Supporting Information, Analytical assay sensitivity) [33, 35, 36, 71–73], as well as the accurate representation of rare events in the dimension-reduced t-SNE map [61, 66, 74], our integrated approach
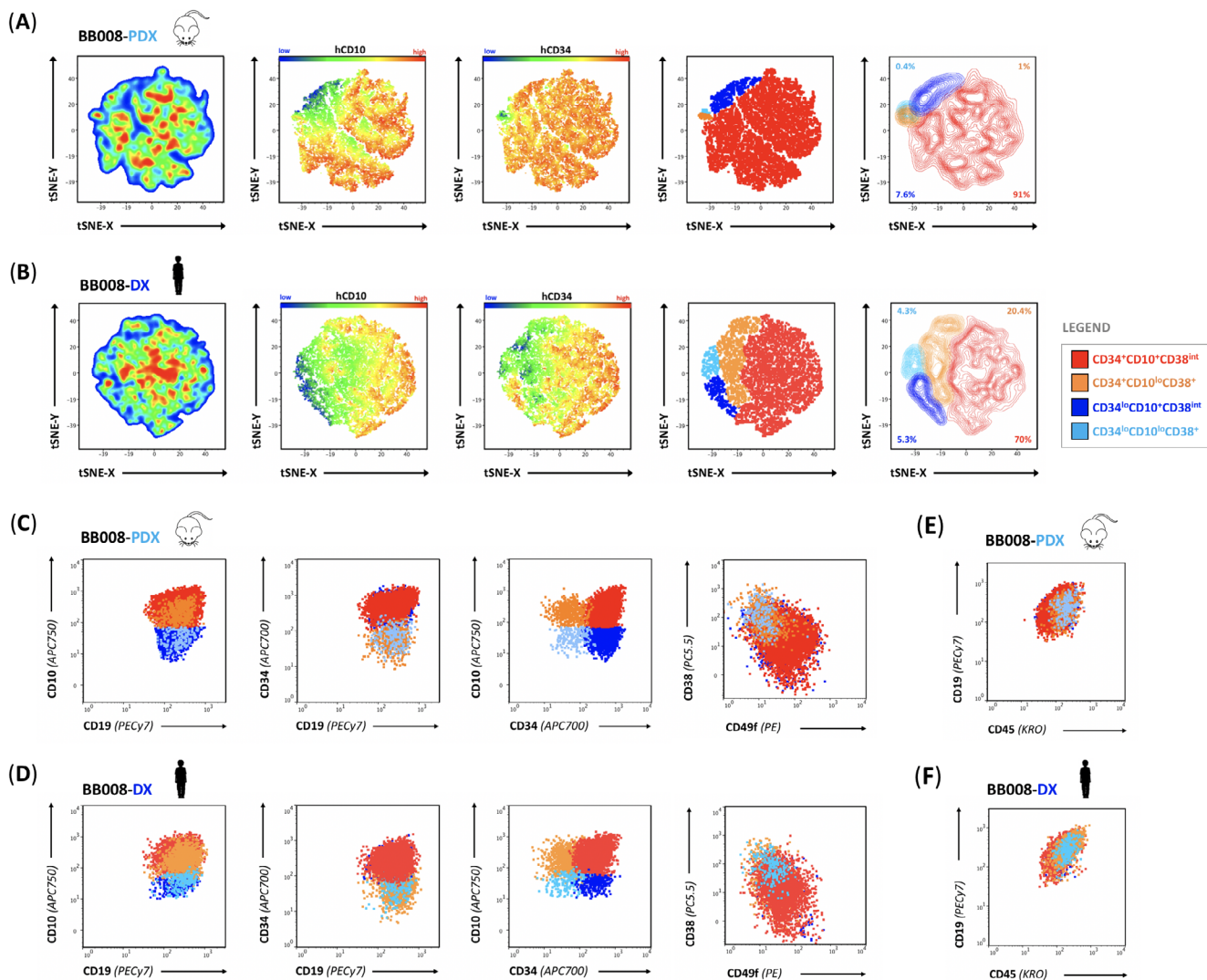

FIGURE 3 High-dimensional gating approach with the unbiased t-SNE algorithm identifies the same subpopulation complexity in patient- and xenograft derived leukemia BB008. (A + B) Application of the automated t-SNE algorithm in standard settings (FlowJo™ 10.4.2) identified the high-dimensional similarities of 30,000 leukemic cells (identical population as in Figure 2), which are visualized in its dimension-reduced space, the t-SNE map, for either (A) DX-patient-derived xenograft (PDX) or (B) the patient (DX), accurately representing rare cell events. After simultaneously assessing staining intensities of all differentially expressed flow markers for each single cell, blasts are separated into spatially resolved populations based on the totality of markers they expressed differentially. Representative t-SNE map visualizations shown (left to right): pseudo-color density plot, heatmap overlays of CD10- or CD34-specific expression intensities, and subpopulation-specific denotations either at the single cell or population level. (C + D) As the unsupervised, multi-dimensional data analysis approach achieved in the t-SNE map eliminates gating biases, the subpopulation characteristics identified with the high-dimensional gating approach were validated by visualizing their unique expression profiles on conventional two-dimensional plots confirming their clear immunophenotypic separation and concise clustering as spatially resolved, distinct subpopulations. The side-by-side comparison between (C) DX-PDX and (D) DX provides a visual validation tool to assess whether the identical phenotypes were independently identified and stably propagated during xenotransplantation. (E + F) At low immunophenotyping depth, all four phenotypically distinct leukemic populations showed indistinguishable CD19/CD45 staining characteristics in both the (E) PDX and (F) patient (DX) [Color figure can be viewed at wileyonlinelibrary.com]

clearly identified very minor subpopulations (≤1%) within the dominant $CD10^+CD34^+CD38^{int}$ leukemic population (91%) (Table S3A).

For the clinical leukemia (DX), where gating precision was even more challenging to achieve with the conventional approach (Figure 2K), our high-dimensional approach reliably discriminated the identical subpopulation complexity in the sample-specific t-SNE map with excellent gating clarity (Figure 3B). Since unbiased t-SNE analysis does not rely on detecting expected phenotypes of known cell populations, the unsupervised discrimination of the same minor phenotypic subpopulations from the patient's identical dominant phenotype confirms that phenotypically stable subpopulations are propagated during xenotransplantation.

3.4 | Cross-validation reveals unique, stable subpopulation expression profiles with additional markers

The phenotypic clarity of the high-dimensionally gated subpopulations becomes apparent when their various marker expressions are visualized on conventional two-dimensional plots, the mainstay of clinical immunophenotyping. Confirmation of their clear immunophenotypic separation and concise clustering on N × N representations is a required cross-validation step in our approach (Supporting Information, Subpopulation criteria). As shown in Figure 3C + D, in both xenograft (PDX) and corresponding patient (DX), each subpopulation maintains a unique expression profile with the inclusion of several additional markers. Notably, when only viewed on CD19/CD45 plots as is common in xenografting studies, the subpopulations remain indistinguishable (Figure 3E + F). These results emphasize the considerable phenotypic heterogeneity of the bulk leukemia population that remains concealed without sufficient immunophenotyping depth and subpopulation-resolving sub-gating (Figure 3C + D). The consistency of the phenotypic patterns between the patient and corresponding PDX illustrates that even at this higher level of marker complexity, the subpopulation-specific expression profiles of the diagnostic leukemia (DX) remain stable after xenotransplantation (PDX).

3.5 | Immunophenotypic shifts in PDX likely reflect differential abundance of phenotypically distinct subpopulations

Our integrated analytical approach reliably discriminated the identical subpopulation complexity in matched samples with excellent gating clarity. To further investigate the mechanism underlying the observed immunophenotypic shifts of the LAIP at the level of the bulk leukemia after xenotransplantation, we next visualized the expression intensities of each marker by creating subpopulation-specific histogram overlays for the PDX and patient (Figure 4A + B). This analysis confirmed the distinct marker profiles of each subpopulation. Notably, significant differences (often >1 log) in expression intensity (Figure 4A) were only detected for markers that contributed to the

observed immunophenotypic shift of the xenotransplanted bulk leukemia depicted in Figure 1B + C. Markers that remained stable on the xenotransplanted bulk population were identically expressed in all identified subpopulations (Figure 4B). This subpopulation-specific pattern was identical between PDX and patient (DX), again confirming the phenotypic stability of the xenotransplanted subpopulations (Figure 4A + B). Our approach also accurately identified the size of each subpopulation within each leukemic population (Figure 4C, Table S3A), revealing their changed abundance levels in the bone marrow after xenotransplantation (Figure 4D). These results suggest that the different abundance levels of phenotypically distinct subpopulations between patient and PDX (Table S3B), rather than a general change in the LAIP of the entire blast population, lead to the observed immunophenotypic shift after xenotransplantation (Figure 1B + C).

3.6 | Xenotransplantation propagates phenotypically stable subpopulations with patient-specific immunophenotypes

To validate the reproducibility and accuracy of our integrated analysis approach, we investigated whether immunophenotypic shifts of the diagnostic leukemia were also observed after xenotransplantation of two other primary pediatric B-ALL cases (Figure 5, Table S1). For BB069 (Figure 5A–F), which progressed to overt leukemia 70 days after xenotransplantation, a complex immunophenotypic shift was again observed (Figure 5A). Our integrated analysis approach reliably discriminated one clearly separated minor subpopulation, with previously unknown immunophenotype, from the dominant population (Figure 5B–D) showing clear phenotypic separation and concise clustering on conventional two-dimensional plots. Subpopulation discrimination was consistently superior on the t-SNE map (Figures 5D and S4A), resulting in more nuanced identification of subpopulations. All subpopulations displayed phenotypic stability in matched samples (Figure 5E). Sample BB035 (Figure 5G–L) only achieved a low, non-progressing leukemic burden (1.4%) in the PDX by 6 months after injection. Even at very low burden (Figure 5G), unbiased t-SNE analysis of nucleated BM singlets reliably identified the minor leukemic infiltration from mouse cell background when stained only with the clinically standardized human B-ALL panel. Of note, engraftment of normal human hematopoietic cells was also absent in this low burden context (Figure S4B). The same t-SNE map (Figure 5G), that precisely discriminated the MRD-level leukemia within mouse BM cells, also accurately identified the same subpopulation complexity (Figures 5H + I and S4C) as in the patient leukemia (Figure 5J + K), demonstrating the high analytical sensitivity of our approach (Table S3C). Finally, as shown in Figure 5F + L, the differential expansion kinetics of the various subpopulations led to different enrichment patterns (Table S3A + B), which impacts the overall phenotypic composition of the leukemia between patient (DX) and PDX. This further supports that the different distributions of phenotypically distinct subpopulations between patient and corresponding PDX lead to the observed immunophenotypic shifts of the bulk leukemia after xenotransplantation.
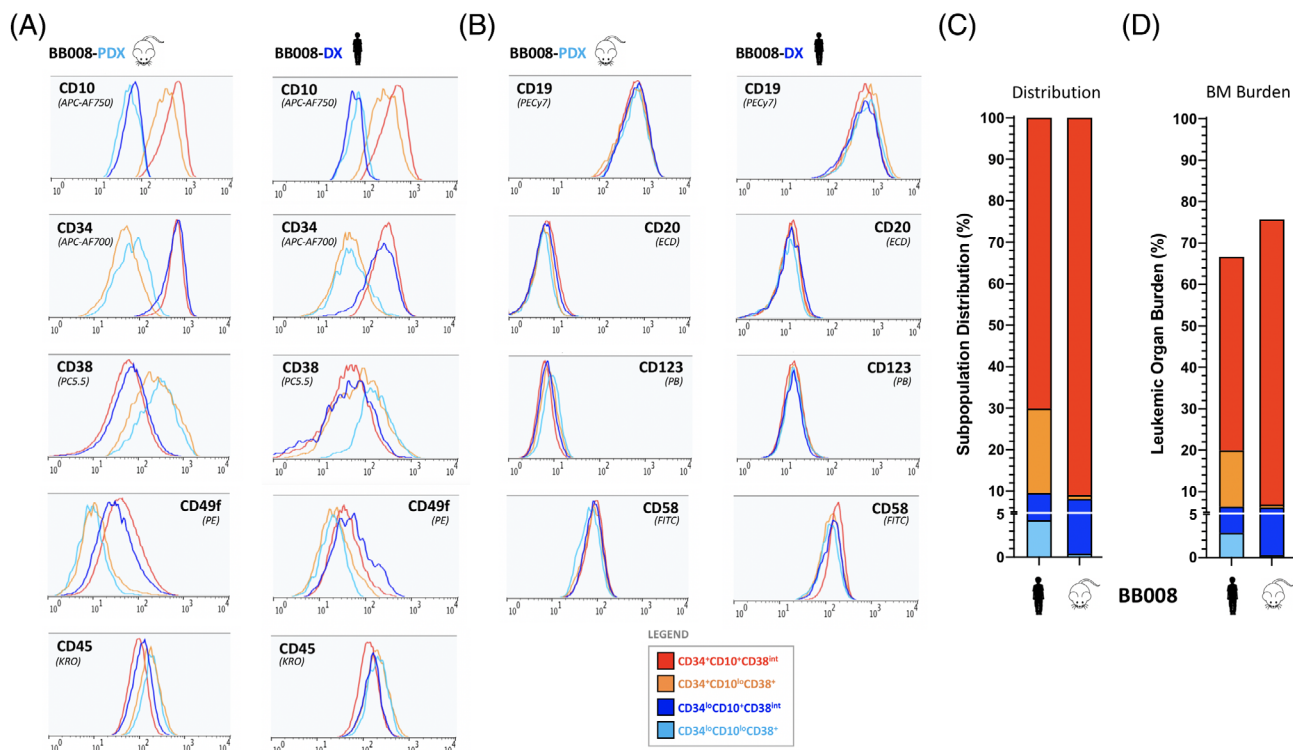
FIGURE 4 Stable phenotypic profiles of subpopulations are identically propagated during xenotransplantation. (A + B) Histogram overlays of all four subpopulations for either the DX-patient-derived xenograft (PDX) or the patient (DX), identically color-coded according to their distinct phenotype. Peak intensities for each phenotypically distinct subpopulation are identical between PDX and patient and revealed additional subpopulation-specific marker complexity when visualized at full immunophenotyping depth, further confirming that phenotypically stable subpopulation complexity is propagated during xenotransplantation. (A) Subpopulations only showed significant differences (often >1 log) in expression intensity for those markers that had similarly shifted for the total leukemic population during xenotransplantation (depicted in Figure 2B, C), while (B) markers that remained stable with xenotransplantation were identically expressed in all identified subpopulations. (C + D) Subpopulations, as identified with our integrated approach and stably propagated during xenotransplantation, are color-coded according to their distinct phenotypes and (C) their relative abundance levels within the diagnostic leukemic population or (D) their respective bone marrow (BM) burden is shown as stacked bar graphs comparing the patient (DX) with the PDX. * Of note, BM burden levels cannot be directly compared between patient and PDX, as the different denominator (mononuclear cells [MNCs] in the patient, nucleated singlets in the PDX) results in lower burden estimates in PDX [Color figure can be viewed at wileyonlinelibrary.com]

4 | DISCUSSION

Despite substantial treatment advances, outcome for patients with relapsed ALL remains poor and patient-specific approaches that could model early disease progression biology and identify relapse-propagating vulnerabilities are in increasing demand [11–13, 75, 76]. Given the poor in vitro viability of patient-derived blasts and limited sample size of diagnostic BM, particularly in children, in vivo expansion of patient-derived blasts in PDX mice have emerged as a powerful tool to facilitate patient-specific leukemia biology studies [29]. Despite phenotypic heterogeneity being a common clinical observation in B-ALL [33, 36, 38–40], the application of in-depth flow cytometry to PDX studies has been limited. In PDX models, it is common practice to confirm human B-ALL engraftment and degree of organ involvement with smaller research flow panels (e.g., anti-human CD45 and lineage-specific CD19) that discriminate their expression on the expanded B-ALL population against a mouse CD45+ staining background. The additional human B-cell maturation markers needed in

clinical diagnostics to discriminate B-ALL blasts from normally maturing counterparts are not necessary for confirming ALL in PDX, due to the paucity of normal human hematopoiesis in mice [14, 22, 24, 28]; but they are occasionally included for certain experimental questions. To determine the value of deeper B-ALL immunophenotyping in the PDX setting, we developed a translational flow cytometry platform (Figure 6) to permit identical assessment of phenotypic heterogeneity and stability of the patient-specific LAIP during xenotransplantation.

The strength of our platform lies in directly combining the rigorous standardization practices and identical phenotyping depth of flow-based clinical diagnostics with the established phenotypic clarity and confirmed leukemogenesis of the xenotransplanted leukemia. The potential impact of different antibody clones, fluorochromes, sample processing and instrument settings on the longitudinal stability and cross-platform comparability of marker expression intensity is a well-known hurdle for accurate and reproducible flow-based assessment [36, 38, 48, 50–56]. By ensuring consistent evaluation of marker expression intensity of clinically validated antibody combinations
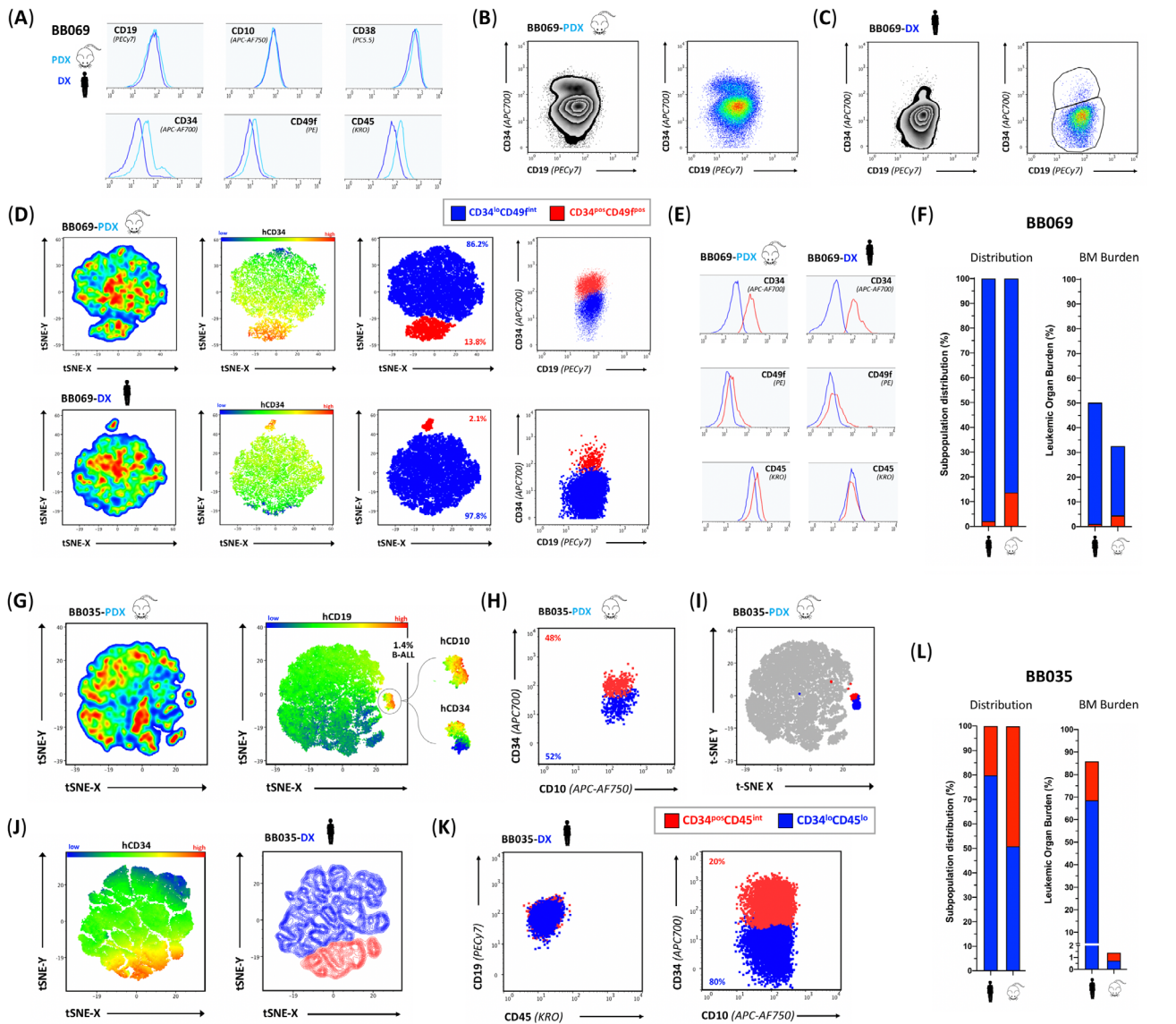
FIGURE 5 Consistent identification and stable propagation of patient-specific subpopulation complexity in two additional pediatric B-ALL cases. (A–L) Two additional pediatric B-ALL cases of matched patient- and PDX-derived diagnostic leukemia, (A–F) BB069 and (G–L) BB035, were identically phenotyped using the same clinical flow protocols with cross-standardized instrument settings. (A–F) Subpopulation complexity in BB069: (A) Histogram overlays of the clinically gated leukemic population from matched samples for BB069 identified a patient-specific complex immunophenotype in the bulk leukemia that shifted after xenotransplantation. (B + C) Density plots (with outliers as dots) of the leukemic population reveal low-frequency information consistent with presence of minor subpopulations (representative CD34/CD19 plot shown). (D) Dimension-reduced t-SNE map of differentially expressed markers in 30,000 blasts; left to right: sample-specific t-SNE map with either pseudo-color density plot, marker-specific heatmap overlay, or subpopulation-specific denotations showing clear phenotypic separation and concise clustering on conventional two-dimensional plots. (E) Histogram overlays of subpopulations confirming phenotypic stability during xenotransplantation. (F) Stacked bar diagram displaying subpopulation-specific distribution in the total leukemic population (left panel) and subpopulation-specific bone marrow (BM) burden (right panel). (G–L) Subpopulation complexity in BB035: (G) Unbiased t-SNE analysis of 30,000 total nucleated bone marrow singlets of DX-PDX reliably separates a small B-ALL infiltration of 1.4% from unstained mouse background and accurately identifies two phenotypically distinct subpopulations, which clear phenotypic separation is confirmed on (H) conventional two-dimensional plots. (I) Manual sequential gating of the leukemic subpopulations achieves less accurate gating clarity at this low level of leukemic infiltration. (J) Dimension-reduced t-SNE map of 30,000 clinically gated leukemic blasts from the patient (DX) separates blasts into spatially separated populations with confirmed phenotypic separation on (K) conventional two-dimensional plots when visualized at high phenotyping depth (right panel) but indistinguishable on basic CD19/CD45 plot (left panel). (L) Stacked bar diagram of subpopulation-specific distribution in the leukemic population (left panel) and subpopulation-specific bone marrow (BM) burden (right panel) emphasizes that both populations only reach measurable residual disease (MRD)-comparable infiltration levels in the PDX. * Of note, BM burden levels (F + L) cannot be directly compared between patient and PDX, as the different denominators (mononuclear cells [MNCs] in the patient, nucleated singlets in the PDX) result in lower burden estimates in PDX [Color figure can be viewed at wileyonlinelibrary.com]
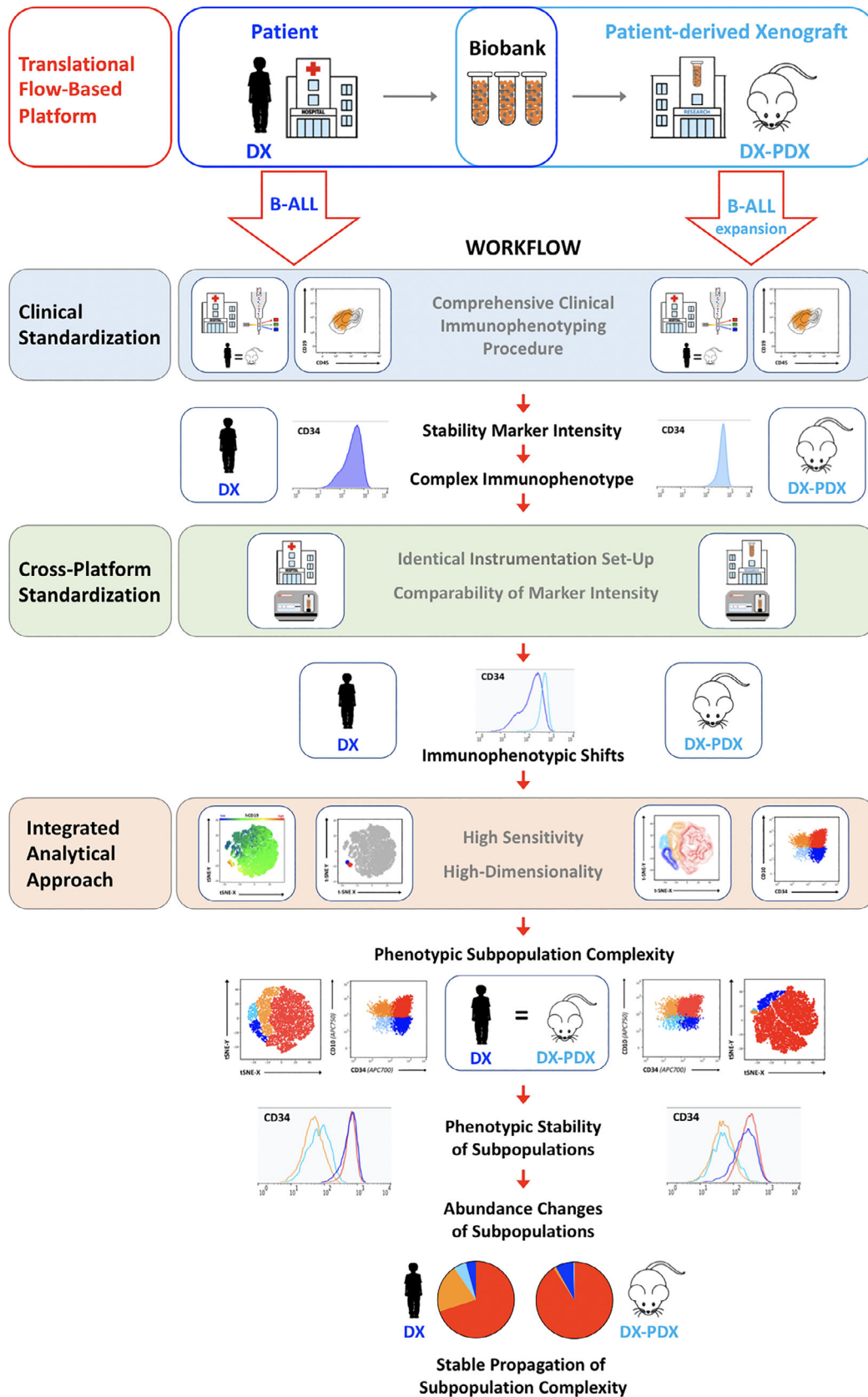
FIGURE 6 Workflow of the translational analytic flow cytometry platform. By utilizing clinically standardized flow protocols with cross-standardized instrument settings to achieve identical phenotyping depth and stable comparability of marker expression intensity across platform, the developed integrated analytical approach accurately and reproducibly identifies subpopulation complexity in both settings facilitating assessment of phenotypic stability across platform [Color figure can be viewed at wileyonlinelibrary.com]

designed to detect a range of B-ALL immunophenotypes amidst normal hematopoiesis, our translational platform meets the technical requirements for accurately detecting and assessing gradual gains and losses of antigens most commonly expressed on B-ALL blasts. The high phenotyping depth and analytical sensitivity of our approach revealed a complex immunophenotype in all xenotransplanted diagnostic B-ALL samples, characterized by heterogeneous expression patterns of several B-cell differentiation antigens on the bulk leukemia, underscoring that the phenotypic heterogeneity of the leukemic population can easily be underestimated with small flow panels commonly used in ALL-PDX models. More importantly, our cross-standardized analysis of matched patient- and PDX-derived samples revealed that the surface marker expression profile of the leukemic population had noticeably changed in PDX mice when compared to the corresponding patient. In each case, the observed immunophenotypic shifts after xenotransplantation were complex and patient-specific, similar to previous reports in patients [32], but in stark contrast to the currently assumed phenotypic stability of the patient leukemia after xenotransplantation [4, 14, 20, 27]. As no markers were lost or gained in any of the analyzed samples, this may explain why immunophenotypic changes after xenotransplantation have not been fully appreciated [4, 14, 19, 20, 27, 28].

The direct comparison of matched patient- and PDX-derived leukemia showed that many markers underwent >1 log fold changes in expression intensity, and were often accompanied by changes in histogram patterns from heterogeneous to homogenous expression or vice versa. These distinct changes mirror the previously reported complex and seemingly uncoordinated phenotypic shifts of the patient's immunophenotype in matched diagnosis-relapse samples when investigated in a clinically standardized manner [32]. However, as we xenotransplanted untreated diagnostic B-ALL samples, chemotherapy-mediated changes to the patient immunophenotype can be excluded for our setting.

It is well known that the multi-dimensionality of complex flow data is challenging to assess when using conventional gating approaches [36, 38, 50, 60–62, 67, 69]. We therefore developed an integrated analytical approach (Figure 6) that utilized unbiased high-dimensional algorithm-based analysis, high analytical sensitivity, and strict subpopulation criteria to resolve phenotypic heterogeneity into subpopulations (Figure 6) [61, 62, 67, 71–73]. This approach identified phenotypically distinct subpopulations as clearly delineated by their high-dimensional population characteristics within the leukemic population in both the patient and PDX. Accurate rare event detection in the dimension-reduced t-SNE maps [61, 66, 68, 74] ensured that even very minor subpopulations (≤1%) were precisely detected as spatially resolved populations in the high-dimensional space, meeting the high analytical sensitivity requirements of our platform. Most importantly, each identified subpopulation showed identical expression patterns between patient and corresponding PDX, which remained stable across the full phenotyping depth. Despite the patient-specific subpopulation complexity, each subpopulation was stably propagated during xenotransplantation, and in each case the dominant population of the patient, irrespective of the specific immunophenotype and

relative abundance in the leukemia, remained dominant in the PDX. However, relative abundance of some subpopulations changed noticeably with xenotransplantation, supporting that the phenotypic shifts observed in longitudinal studies may reflect the different enrichment pattern of distinct minor subpopulations rather than a general plasticity of marker expressions on the bulk population.

Given the clinical and translational importance of subclonal complexity in ALL disease progression [1–10], it is important to be able to distinguish therapy-resistant and potentially relapse-driving clones as viable cell populations within the leukemic population both in xenografts and in patients [47]. The demonstrated phenotypic stability of engrafted subpopulations from each patient's untreated diagnostic BM could be a significant step to achieving this goal. Our translational flow cytometry platform and integrated analytical approach, therefore, address an important gap in studying phenotypic subpopulation complexity in PDX models. Our data show the importance of ensuring the cross-standardized assessment of phenotypic heterogeneity of the leukemic population in matched samples at the single-cell level, so that patient-specific subpopulation complexity can be resolved. In conclusion, we here provide an adaptable translational flow cytometry method that can be integrated into various PDX models and help to further unravel disease complexity at the phenotypic level [60, 62]. By incorporating high-resolution identification of phenotypically distinct subpopulations, this novel analytical platform could greatly expand the utility of PDX for investigating ALL disease progression biology.

AUTHOR CONTRIBUTIONS

Lorraine Liu: Formal analysis; methodology; software; validation; writing-review & editing. **Angela Tsang:** Formal analysis; methodology; software; validation; writing-review & editing. **Philipp Lange:** Funding acquisition; methodology; resources; writing-review & editing. **C Lim:** Funding acquisition; methodology; resources; writing-review & editing. **Christopher Maxwell:** Funding acquisition; methodology; resources; writing-review & editing. **Suzanne Vercauteren:** Data curation; formal analysis; funding acquisition; investigation; methodology; project administration; resources; software; supervision; validation; writing-review & editing. **Gregor Reid:** Conceptualization; formal analysis; funding acquisition; investigation; methodology; project administration; resources; software; supervision; validation;

visualization; writing-original draft; writing-review & editing. **Nina Rolf:** Conceptualization; formal analysis; funding acquisition; investigation; methodology; project administration; resources; software; supervision; validation; visualization; writing-original draft; writing-review & editing.

CONFLICT OF INTEREST

The authors declare no competing financial interests.

ORCID

Nina Rolf https://orcid.org/0000-0002-4531-2994
Lorraine Y. T. Liu https://orcid.org/0000-0001-5191-3131
Angela Tsang https://orcid.org/0000-0001-7968-8052
Philipp F. Lange https://orcid.org/0000-0003-1171-5864
Chinten James Lim https://orcid.org/0000-0001-6381-7585
Christopher A. Maxwell https://orcid.org/0000-0002-0713-7136
Suzanne M. Vercauteren https://orcid.org/0000-0003-2224-0307
Gregor S. D. Reid https://orcid.org/0000-0002-7567-3424

REFERENCES

1. Anderson K, Lutz C, Van Delft FW, Bateman CM, Guo Y, Colman SM, et al. Genetic variegation of clonal architecture and propagating cells in leukaemia. Nature. 2011;469:356–61.
2. Waanders E, Gu Z, Dobson SM, Antić Ž, Crawford JC, Ma X, et al. Mutational landscape and patterns of clonal evolution in relapsed pediatric acute lymphoblastic Leukemia. Blood Cancer Discov. 2020; 1:96–111.
3. Ma X, Edmonson M, Yergeau D, Muzny DM, Hampton OA, Rusch M, et al. Rise and fall of subclones from diagnosis to relapse in pediatric B-acute lymphoblastic leukaemia. Nat Commun. 2015;6:6604.
4. Notta F, Mullighan CG, Wang JCYY, Poeppl A, Doulatov S, Phillips LA, et al. Evolution of human BCR–ABL1 lymphoblastic leukaemia-initiating cells. Nature. 2011;469:362–7.
5. Jan M, Majeti R. Clonal evolution of acute leukemia genomes. Oncogene. 2013;32:135–40.
6. Mullighan CG, Phillips LA, Su X, Ma J, Miller CB, Shurtleff SA, et al. Genomic analysis of the clonal origins of relapsed acute lymphoblastic leukemia. Science. 2008;322:1377–80.
7. Choi S, Henderson MJ, Kwan E, Beesley AH, Sutton R, Bahar AY, et al. Relapse in children with acute lymphoblastic leukemia involving selection of a preexisting drug-resistant subclone. Blood. 2007;110: 632–9.
8. Dobson SM, García-Prat L, Vanner RJ, Wintersinger J, Waanders E, Gu Z, et al. Relapse-fated latent diagnosis subclones in acute B lineage leukemia are drug tolerant and possess distinct metabolic programs. Cancer Discov. 2020;10:568–87.
9. Landau DA, Carter SL, Getz G, Wu CJ. Clonal evolution in hematological malignancies and therapeutic implications. Leukemia. 2014;28: 34–43.
10. Henderson MJ, Choi S, Beesley AH, Sutton R, Venn NC, Marshall GM, et al. Mechanism of relapse in pediatric acute lymphoblastic leukemia. Cell Cycle. 2008;7:1315–20.
11. Bhojwani D, Pui C-H. Relapsed childhood acute lymphoblastic leukaemia. Lancet Oncol. 2013;14:e205–17.
12. Malard F, Mohty M. Acute lymphoblastic leukaemia. Lancet. 2020; 395:1146–62.
13. Inaba H, Mullighan CG. Pediatric acute lymphoblastic leukemia. Haematologica. 2020;105:2524–39.
14. le Viseur C, Hotfilder M, Bomken S, Wilson K, Röttgers S, Schrauder A, et al. In childhood acute lymphoblastic leukaemia, blasts

at different stages of immunophenotypic maturation have stem cell properties. Cancer Cell. 2008;14:47–58.
15. Furness CL, Mansur MB, Weston VJ, Ermini L, van Delft FW, Jenkinson S, et al. The subclonal complexity of STIL-TAL1+ T-cell acute lymphoblastic leukaemia. Leukemia. 2018;32:1984–93.
16. Hong D, Gupta R, Ancliff P, Atzberger A, Brown J, Soneji S, et al. Initiating and cancer-propagating cells in TEL-AML1-associated childhood leukemia. Science. 2008;319:336–9.
17. Jones L, Carol H, Evans K, Richmond J, Houghton PJ, Smith MA, et al. A review of new agents evaluated against pediatric acute lymphoblastic leukemia by the pediatric Preclinical Testing Program. Leukemia. 2016;30:2133–41.
18. Clappier E, Gerby B, Sigaux F, Delord M, Touzri F, Hernandez L, et al. Clonal selection in xenografted human T cell acute lymphoblastic leukemia recapitulates gain of malignancy at relapse. J Exp Med. 2011; 208:653–61.
19. Wang K, Sanchez-Martin M, Wang X, Knapp KM, Koche R, Vu L, et al. Patient-derived xenotransplants can recapitulate the genetic driver landscape of acute leukemias. Leukemia. 2017;31:151–8.
20. Schmitz M, Breithaupt P, Scheidegger N, Cario G, Bonapace L, Meissner B, et al. Xenografts of highly resistant leukemia recapitulate the clonal composition of the leukemogenic compartment. Blood. 2011;118:1854–64.
21. Rehe K, Wilson K, Bomken S, Williamson D, Irving J, den Boer ML, et al. Acute B lymphoblastic leukaemia-propagating cells are present at high frequency in diverse lymphoblast populations. EMBO Mol Med. 2013;5:38–51.
22. Woiterski J, Ebinger M, Witte KE, Goecke B, Heininger V, Philippek M, et al. Engraftment of low numbers of pediatric acute lymphoid and myeloid leukemias into NOD/SCID/IL2Rcγnull mice reflects individual leukemogenecity and highly correlates with clinical outcome. Int J Cancer. 2013;133:1547–56.
23. Vormoor HJ. Malignant stem cells in childhood acute lymphoblastic leukemia: the stem cell concept revisited. Cell Cycle. 2009;8:996–9.
24. Barrett DM, Seif AE, Carpenito C, Teachey DT, Fish JD, June CH, et al. Noninvasive bioluminescent imaging of primary patient acute lymphoblastic leukemia: a strategy for preclinical modeling. Blood. 2011;118:e112–7.
25. Patel B, Dey A, Castleton AZ, Schwab C, Samuel E, Sivakumaran J, et al. Mouse xenograft modeling of human adult acute lymphoblastic leukemia provides mechanistic insights into adult LIC biology. Blood. 2014;124:96–105.
26. Elder A, Bomken S, Wilson I, Blair HJ, Cockell S, Ponthan F, et al. Abundant and equipotent founder cells establish and maintain acute lymphoblastic leukaemia. Leukemia. 2017;31:2577–86.
27. Richter-Pechańska P, Kunz JB, Bornhauser B, Knebel Doeberitz C, Rausch T, Erarslan-Uysal B, et al. PDX models recapitulate the genetic and epigenetic landscape of pediatric T-cell leukemia. EMBO Mol Med. 2018;10:1–13.
28. Meyer LH, Debatin K-M. Diversity of human leukemia xenograft mouse models: implications for disease biology. Cancer Res. 2011;71: 7141–4.
29. Hidalgo M, Amant F, Biankin AV, Budinská E, Byrne AT, Caldas C, et al. Patient-derived xenograft models: an emerging platform for translational cancer research. Cancer Discov. 2014;4:998–1013.
30. Uzozie AC, Ergin E, Rolf N, Tsui J, Lorentzian A, Weng SS, et al. PDX models reflect the proteome landscape of pediatric acute lymphoblastic leukemia but divert in select pathways. J Exp Clin Cancer Res. 2021;40:96.
31. Erarslan-Uysal B, Kunz JB, Rausch T, Richter-Pechańska P, Belzen IA, Frismantas V, et al. Chromatin accessibility landscape of pediatric T-lymphoblastic leukemia and human T-cell precursors. EMBO Mol Med. 2020;12:1–14.
32. Borowitz MJ, Pullen DJ, Winick N, Martin PL, Bowman WP, Camitta B. Comparison of diagnostic and relapse flow cytometry

phenotypes in childhood acute lymphoblastic leukemia: implications for residual disease detection: a report from the Children's Oncology Group. Cytometry B Clin Cytom. 2005;68:18–24.

33. Wood BL. Principles of minimal residual disease detection for hematopoietic neoplasms by flow cytometry. Cytometry B Clin Cytom. 2016;90:47–53.

34. van Lochem EG, van der Velden VHJ, Wind HK, te Marvelde JG, Westerdaal NAC, van Dongen JJM. Immunophenotypic differentiation patterns of normal hematopoiesis in human bone marrow: reference patterns for age-related changes and disease-induced shifts. Cytometry. 2004;60B:1–13.

35. Theunissen P, Mejstrikova E, Sedek L, van der Sluijs-Gelling AJ, Gaipa G, Bartels M, et al. Standardized flow cytometry for highly sensitive MRD measurements in B-cell acute lymphoblastic leukemia. Blood. 2017;129:347–57.

36. van Dongen JJM, Lhermitte L, Böttcher S, Almeida J, van der Velden VHJ, Flores-Montero J, et al. EuroFlow antibody panels for standardized n-dimensional flow cytometric immunophenotyping of normal, reactive and malignant leukocytes. Leukemia. 2012;26: 1908–75.

37. Gaipa G, Basso G, Aliprandi S, Migliavacca M, Vallinoto C, Maglia O, et al. Prednisone induces immunophenotypic modulation of CD10 and CD34 in nonapoptotic B-cell precursor acute lymphoblastic leukemia cells. Cytometry B Clin Cytom. 2008;74B:150–5.

38. Dworzak MN, Buldini B, Gaipa G, Ratei R, Hrusak O, Luria D, et al. AIEOP-BFM consensus guidelines 2016 for flow cytometric immunophenotyping of Pediatric acute lymphoblastic leukemia. Cytometry B Clin Cytom. 2018;94:82–93.

39. Øbro NF, Marquart HV, Madsen HO, Ryder LP, Andersen MK, Lausen B, et al. Immunophenotype-defined sub-populations are common at diagnosis in childhood B-cell precursor acute lymphoblastic leukemia. Leukemia. 2011;25:1652–7.

40. Wood BL, Arroz M, Barnett D, DiGiuseppe J, Greig B, Kussick SJ, et al. 2006 Bethesda International Consensus recommendations on the immunophenotypic analysis of hematolymphoid neoplasia by flow cytometry: optimal reagents and reporting for the flow cytometric diagnosis of hematopoietic neoplasia. Cytometry B Clin Cytom. 2007; 72(Suppl 1):S14–22.

41. Chen X, Wood BL. Monitoring minimal residual disease in acute leukemia: technical challenges and interpretive complexities. Blood Rev. 2017;31:63–75.

42. Dworzak MN, Gaipa G, Schumich A, Maglia O, Ratei R, Veltroni M, et al. Modulation of antigen expression in B-cell precursor acute lymphoblastic leukemia during induction therapy is partly transient: evidence for a drug-induced regulatory phenomenon. Results of the AIEOP-BFM-ALL-FLOW-MRD-study group. Cytometry B Clin Cytom. 2010;78:147–53.

43. DiGiuseppe JA, Fuller SG, Borowitz MJ. Overexpression of CD49f in precursor B-cell acute lymphoblastic leukemia: potential usefulness in minimal residual disease detection. Cytometry B Clin Cytom. 2009; 76:150–5.

44. Coustan-Smith E, Song G, Clark C, Key L, Liu P, Mehrpooya M, et al. New markers for minimal residual disease detection in acute lymphoblastic leukemia. Blood. 2011;117:6267–76.

45. Lang F, Wojcik B, Bothur S, Knecht C, Falkenburg JHF, Schroeder T, et al. Plastic CD34 and CD38 expression in adult B–cell precursor acute lymphoblastic leukemia explains ambiguity of leukemia-initiating stem cell populations. Leukemia. 2017;31:731–4.

46. van Dongen JJM, van der Velden VHJ, Bruggemann M, Orfao A. Minimal residual disease diagnostics in acute lymphoblastic leukemia: need for sensitive, fast, and standardized technologies. Blood. 2015; 125:3996–4009.

47. Luskin MR, Murakami MA, Manalis SR, Weinstock DM. Targeting minimal residual disease: a path to cure? Nat Rev Cancer. 2018;18: 255–63.

48. Maecker HT, McCoy JP, Nussenblatt R. Standardizing immunophenotyping for the Human Immunology Project. Nat Rev Immunol. 2012;12:191–200.

49. Böttcher S, van der Velden VHJ, Villamor N, Ritgen M, Flores-Montero J, Escobar HM, et al. Lot-to-lot stability of antibody reagents for flow cytometry. J Immunol Methods. 2017;475:112294. https://doi.org/10.1016/j.jim.2017.03.018.

50. Finak G, Langweiler M, Jaimes M, Malek M, Taghiyar J, Korin Y, et al. Standardizing flow cytometry immunophenotyping analysis from the Human Immunophenotyping Consortium. Sci Rep. 2016;6:20686.

51. Kalina T, Flores-Montero J, van der Velden VHJ, Martin-Ayuso M, Böttcher S, Ritgen M, et al. EuroFlow standardization of flow cytometer instrument settings and immunophenotyping protocols. Leukemia. 2012;26:1986–2010.

52. Davis BH, Dasgupta A, Kussick S, Han J-Y, Estrellado A, ICSH/ICCS Working Group. Validation of cell-based fluorescence assays: practice guidelines from the ICSH and ICCS - part II - preanalytical issues. Cytometry B Clin Cytom. 2013;84:286–90.

53. Tanqri S, Vall H, Kaplan D, Hoffman B, Purvis N, Porwit A, et al. Validation of cell-based fluorescence assays: practice guidelines from the ICSH and ICCS - part III - analytical issues. Cytometry B Clin Cytom. 2013;84:291–308.

54. Barnett D, Louzao R, Gambell P, De J, Oldaker T, Hanson CA, et al. Validation of cell-based fluorescence assays: practice guidelines from the ICSH and ICCS - part IV - postanalytic considerations. Cytometry B Clin Cytom. 2013;84:309–14.

55. Wood B, Jevremovic D, Béné MC, Yan M, Jacobs P, Litwin V, et al. Validation of cell-based fluorescence assays: practice guidelines from the ICSH and ICCS - part V - assay performance criteria. Cytometry B Clin Cytom. 2013;84:315–23.

56. Cossarizza A, Chang HD, Radbruch A, Acs A, Adam D, Adam-Klages S, et al. Guidelines for the use of flow cytometry and cell sorting in immunological studies (second edition). Eur J Immunol. 2019;49:1457–973.

57. Theunissen PMJ, Sedek L, De Haas V, Szczepanski T, Van Der Sluijs A, Mejstrikova E, et al. Detailed immunophenotyping of B-cell precursors in regenerating bone marrow of acute lymphoblastic leukaemia patients: implications for minimal residual disease detection. Br J Haematol. 2017;178:257–66.

58. Lutz C, Woll PS, Hall G, Castor a, Dreau H, Cazzaniga G, et al. Quiescent leukaemic cells account for minimal residual disease in childhood lymphoblastic leukaemia. Leukemia. 2013;27:1204–7.

59. Trentin L, Queudeville M, Eckhoff SM, Hasan N, Münch V, Boldrin E, et al. Leukemia reconstitution in vivo is driven by cells in early cell cycle and low metabolic state. Haematologica. 2018;103:1008–17.

60. O'Donnell EA, Ernst DN, Hingorani R. Multiparameter flow cytometry: advances in high resolution analysis. Immune Netw. 2013;13:43–54.

61. Mair F, Hartmann FJ, Mrdjen D, Tosevski V, Krieg C, Becher B. The end of gating? An introduction to automated analysis of high dimensional cytometry data. Eur J Immunol. 2016;46:34–43.

62. Palit S, Heuser C, De Almeida GP, Theis FJ, Zielinski CE. Meeting the challenges of high-dimensional single-cell data analysis in immunology. Front Immunol. 2019;10:1–12.

63. Schuurhuis GJ, Heuser M, Freeman S, Béné M-C, Buccisano F, Cloos J, et al. Minimal/measurable residual disease in AML: a consensus document from the European LeukemiaNet MRD Working Party. Blood. 2018;131:1275–91.

64. van Lochem EG, Wiegers YM, van den Beemd R, Hahlen K, van Dongen JJ, Hooijkaas H. Regeneration pattern of precursor-B-cells in bone marrow of acute lymphoblastic leukemia patients depends on the type of preceding chemotherapy. Leukemia. 2000;14:688–95.

65. Gaipa G, Basso G, Maglia O, Leoni V, Faini A, Cazzaniga G, et al. Drug-induced immunophenotypic modulation in childhood ALL: implications for minimal residual disease detection. Leukemia. 2005;19: 49–56.

66. Amir ED, Davis KL, Tadmor MD, Simonds EF, Levine JH, Bendall SC, et al. viSNE enables visualization of high dimensional single-cell data and reveals phenotypic heterogeneity of leukemia. Nat Biotechnol. 2013;31:545–52.

67. Saeys Y, Van Gassen S, Lambrecht BN. Computational flow cytometry: helping to make sense of high-dimensional immunology data. Nat Rev Immunol. 2016;16:449–62.

68. Van Der Maaten LJP, Hinton GE. Visualizing high-dimensional data using t-sne. J Mach Learn Res. 2008;9:2579–605.

69. Cheung M, Campbell JJ, Whitby L, Thomas RJ, Braybrook J, Petzing J. Current trends in flow cytometry automated data analysis software. Cytom Part A. 2021. https://doi.org/10.1002/cyto.a.24320.

70. Chester C, Maecker HT. Algorithmic tools for mining high-dimensional cytometry data. J Immunol. 2015;195:773–9.

71. Hedley BD, Keeney M. Technical issues: flow cytometry and rare event analysis. Int J Lab Hematol. 2013;35:344–50.

72. Arroz M, Came N, Lin P, Chen W, Yuan C, Lagoo A, et al. Consensus guidelines on plasma cell myeloma minimal residual disease analysis and reporting. Cytometry B Clin Cytom. 2016;90:31–9.

73. Sommer U, Eck S, Marszalek L, Stewart JJ, Bradford J, McCloskey TW, et al. High-sensitivity flow cytometric assays: considerations for design control and analytical validation for identification of rare events. Cytometry B Clin Cytom. 2021;100:42–51.

74. DiGiuseppe JA, Tadmor MD, Pe'er D. Detection of minimal residual disease in B lymphoblastic leukemia using viSNE. Cytometry B Clin Cytom. 2015;88:294–304.

75. Raetz EA, Bhatla T. Where do we stand in the treatment of relapsed acute lymphoblastic leukemia? Hematology Am Soc Hematol Educ Program. 2012;2012:129–36.

76. Berry DA, Zhou S, Higley H, Mukundan L, Fu S, Reaman GH, et al. Association of minimal residual disease with clinical outcome in pediatric and adult acute lymphoblastic leukemia: a meta-analysis. JAMA Oncol. 2017;3:e170580.

SUPPORTING INFORMATION

Additional supporting information may be found online in the Supporting Information section at the end of this article.